Published in final edited form as:
Cell Metab. 2010 January ; 11(1): 58–69. doi:10.1016/j.cmet.2009.11.009.

Sarcolemmal ATP-sensitive K+ channels control energy expenditure determining body weight

Alexey E. Alekseev[1,*], **Santiago Reyes**[1], **Satsuki Yamada**[1], **Denice M. Hodgson-Zingman**[1,2], **Srinivasan Sattiraju**[1], **Zhiyong Zhu**[2], **Ana Sierra**[2], **Marina Gerbin**[1], **William A. Coetzee**[3], **David J. Goldhamer**[4], **Andre Terzic**[1], and **Leonid V. Zingman**[1,2]

[1]Marriott Heart Diseases Research Program, Division of Cardiovascular Diseases, Department of Medicine, Department of Molecular Pharmacology and Experimental Therapeutics and Department of Medical Genetics, Mayo Clinic, 200 First Street SW, Rochester, Minnesota 55905, USA

[2]Department of Internal Medicine, University of Iowa, Carver College of Medicine, 285 Newton Rd., CBRB2296, Iowa City, Iowa 52242 USA

[3]Department of Pediatrics, NYU School of Medicine, 560 First Avenue TCH-521, New York, New York 10016, USA

[4]The Center for Regenerative Biology, Department of Molecular and Cell Biology, Advanced Technology Laboratory, University of Connecticut, 1392 Storrs Road Unit 4243, Storrs, Connecticut 06269, USA

Summary

Metabolic processes that regulate muscle energy use are major determinants of bodily energy balance. Here we find that sarcolemmal ATP-sensitive K^+ (K_{ATP}) channels, which couple membrane excitability with cellular metabolic pathways, set muscle energy expenditure under physiological stimuli. Disruption of K_{ATP} channel function provoked, in conditions of unaltered locomotor activity and blood substrate availability, an extra energy cost of cardiac and skeletal muscle performance. Inefficient fuel metabolism in K_{ATP} channel-deficient striated muscles reduced glycogen and fat body depots promoting a lean phenotype. The propensity to lesser body weight imposed by K_{ATP} channel deficit persisted under a high-fat diet, yet obesity restriction was achieved at the cost of compromised physical endurance. Thus, sarcolemmal K_{ATP} channels govern muscle energy economy, and their down-regulation in a tissue-specific manner could present an anti-obesity strategy by rendering muscle increasingly thermogenic at rest and less fuel efficient during exercise.

Body weight reflects the balance between energy intake and consumption. Biological systems have evolved in an environment with ample demand for physical activity and restricted food supply presenting a selection bias for mechanisms that conserve energy (Celi, 2009). While naturally protective, however, these energy conserving systems under conditions of hyperalimentation and sedentary lifestyle promote obesity (Schwartz et al., 2003; Ogden et al., 2006). Hence, comprehension of energy conserving mechanisms and interference with their efficiency could advance obesity treatment and prevention.

*Correspondence should be addressed to: alekseev.alexey@mayo.edu, Tel: 507 284-9501/FAX: 507 266-9936 or leonid-zingman@uiowa.edu, Tel: 319 384-2917/FAX 319 353-5552.

The ATP-sensitive K^+ (K_{ATP}) channel, due to a unique ability to integrate energy cues with membrane excitability-dependent processes, may represent such an energy controlling mechanism (Miki and Seino, 2005; Ashcroft, 2005; Alekseev et al., 2005; Nichols, 2006). Widely expressed in excitable tissues, K_{ATP} channels are formed by tissue-specific multimerization of pore-forming Kir6.x with regulatory SURx subunits (Inagaki et al., 1995; Yamada et al., 1997; Babenko et al., 1998), yet their adenine nucleotide sensing function remains consistent throughout the body (Nichols et al., 1996; Aguilar-Bryan et al., 2001; Ashcroft, 2005; Zingman et al., 2003).

Sarcolemmal K_{ATP} channels (Kir6.2/SUR2A) are increasingly recognized as safety valves protecting muscle function under stress (Matar et al., 2000; Zingman et al., 2002; Renaud, 2002; Kane et al., 2004; Miki and Seino, 2005; Nichols, 2006). In response to stress-induced modulation of intracellular nucleotide levels (Nichols and Lederer, 1991; Miki and Seino, 2005), K_{ATP} channel opening limits the duration or amplitude of cardiac and skeletal muscle action potentials, reducing Na^+/K^+-, Ca^{2+}- and myosin-ATPase operation to prevent energy depletion (Zingman et al., 2002; Thabet et al., 2005; Cifelli et al., 2007, 2008). While skeletal and cardiac muscles account for 10–20% of sedentary daily energy use, during physical activity their energy consumption increases 20–100 times over basal levels (McArdle et al., 1996). Therefore, by integrating with the intracellular energy network (Weiss and Lamp, 1989; Nichols and Lederer, 1990; Carrasco et al., 2001; Abraham et al., 2002; Selivanov et al., 2004), K_{ATP} channels may set the performance of cellular energy-sparing systems and control muscle energy expenditure not only under stress conditions but at any level of activity.

Here, genetic disruption of K_{ATP} channel function was found to raise energy expenditure in cardiac and skeletal muscles, generating a lean phenotype resistant to diet-induced obesity albeit with compromised physical endurance. The K_{ATP} channel is thus identified as a safeguard of bodily energy economy, mapping a molecular regulator of obesity risk.

RESULTS

K_{ATP} channel-dependent control of body weight

Mice lacking K_{ATP} channels (Kir6.2-KO), individually housed and fed *ad libitum* with regular chow diet, demonstrated lower body weights than age- and gender-matched wild-type (WT; see Experimental Procedures). Compared to WT, until 4 months of age, Kir6.2-KO had similar body weight and fat distribution (Figure 1B and 1E–G), as well as adipose tissue-related endocrine status (Figure S1). Divergence in body weight was manifested at 20 weeks of age, and was maintained throughout the 50-week follow-up (Figure 1A and 1B). The reduced body weight in Kir6.2-KO was not a consequence of altered growth, as both cohorts displayed similar heights and reached 12.2±0.2 cm (n=10) for Kir6.2-KO and 12.4±0.1 cm (n=10) for WT by 12 months of age. As a result, the body mass index and waist-to-height ratio of Kir6.2-KO were significantly reduced compared to WT (Figure 1C and 1D). Whole body magnetic resonance imaging (MRI) indicated that the lower body weight of 1-year old Kir6.2-KO was associated with depletion of subcutaneous and abdominal fat depots (Figure 1E–1G). Thus, the mature Kir6.2-KO demonstrated a phenotype characterized by low body weight and reduced fat storage, suggesting an altered balance between energy availability and consumption induced by K_{ATP} channel gene knockout.

Augmented energy expenditure underlies K_{ATP} channel-deficient lean phenotype

To assess K_{ATP} channel-dependent regulation of energy balance, Kir6.2-KO and WT mice were studied at the age of 3–4 months when effects of senescence or differences in adiposity could be excluded. Locomotor activity, compared by telemetry, was indistinguishable between cohorts (Figure 2A). Analysis of motion patterns, accumulated during day cycles, revealed

equivalent dwell times at rest (Figure 2B) and comparable time periods at all levels of detected activity (Figure 2C) for WT and Kir6.2-KO. Specifically, the in-action pattern was analyzed as a memory-less Poisson process, with the time spent at activity level *k* proportional to $e^{-\alpha k}$, where the mean characteristic level of activity ($1/\alpha$) was 27.9±0.8 movements/min for WT and 27.1±0.9 movements/min for Kir6.2-KO (n=8 in each group; Figure 2C). Kir6.2-KO had an elevated calory intake from food, cumulatively measured during 24 h and corrected for body weight (Figure 2D). Blood samples revealed similar glucose, triglyceride and free fatty acid concentrations in WT and Kir6.2-KO (Figure S1) indicating equal energy substrate availability for tissue uptake, excluding disproportional energy supply as a basis for distinct trends in body weight.

Equal body weight, under comparable levels of activity and elevated caloric input, suggests raised energy expenditure (EE). During continuous 24-h monitoring under sedentary conditions indirect calorimetry revealed a higher rate of O_2 consumption in Kir6.2-KO compared to WT (Figure 2E). Concomitantly, Kir6.2-KO demonstrated a higher rate of caloric output normalized to whole body weight, during day periods, reflecting increased EE compared to WT (Figure 2F). The higher caloric output in Kir6.2-KO was associated with an elevated rate of carbohydrate consumption relative to WT, and equal rates of lipid use (Figure 2E), estimated using Ferrannini's equations (Ferrannini, 1988). Cumulative carbohydrate utilization in Kir6.2-KO during each 12-h day period, was 4.5–5 g per kg of weight above that of WT (Figure 2G). Assuming a 4 kcal energy yield from 1 g of carbohydrates, this would account for an additional 1.5–1.6 kcal/kg/h EE measured in Kir6.2-KO (Figure 2F).

Under sedentary conditions, EE comprises basal metabolic rate and thermogenesis aimed at non-exercise activity such as upholding posture, fidgeting and involuntary muscle contraction (Levine et al., 1999). To evaluate the contribution of K_{ATP} channels to the energy cost of physical activity, indirect calorimetry was further performed under a low exercise regimen that imposed walking on a treadmill runway. Upon acquisition of baseline EE during sleep, treadmill speed was adjusted to body weight to achieve a workload rate of 2×10^{-3} Joules/s (2 mW) at 5° inclination. In response to initiation of exercise both WT and Kir6.2-KO displayed a transient, ~10 min-long, stress-induced elevation of O_2 consumption rates until matching the imposed workload at steady-state (Figure 2H). With exception of the first 2 min, when activation of aerobic metabolism in Kir6.2-KO was delayed relative to WT, a deficit in K_{ATP} channel function resulted in increased steady-state EE along with elevated rates of carbohydrate and lipid utilization (Figure 2H). Subtraction of baseline from steady-state EE defined the 2 mW activity-specific component, which was significantly higher in Kir6.2-KO than WT (n=8 in each group; $p<0.05$, Figure 2I). K_{ATP} channel deficit thus raises EE through an extra energy cost of physical activity.

K_{ATP} channels determine EE in muscle tissues governing body energy stores

The main determinant of activity-related energy cost is the performance of skeletal and cardiac muscles (Kunz, 2001; Ghanassia et al., 2007). To dissect K_{ATP} channel-dependent regulation of skeletal muscle EE, the transgenic Tg[MyoD-Kir6.1AAA] model lacking channel function in a tissue-specific manner was developed (Figure 3A and 3B). Crossing Tg[CX1-eGFP-Kir6.1AAA] mice, which express eGFP in all somatic cells (Figure 3A, upper panel) but are otherwise phenotypically normal (Malester et al, 2007), with MyoD-cre transgenic animals (Chen et al., 2005) generated Tg[MyoD-Kir6.1AAA] progeny with skeletal muscle-specific Kir6.1AAA transgene expression tracked by selective elimination of eGFP fluorescence (Figure 3A, lower panel). Accordingly, patch-clamp recordings demonstrated lack of K_{ATP} channel activity in skeletal myofibers isolated from Tg[MyoD-Kir6.1AAA] in response to the potassium channel opener pinacidil or to metabolic challenge initiated by the mitochondria uncoupler 2,4-dinitrophenol (Figure 3B). Skeletal muscle-specific ablation of K_{ATP} channel

function resulted in an elevated cost of physical activity, estimated by subtraction of baseline EE from the 2 mW steady-state EE, in Tg[MyoD-Kir6.1AAA] compared to littermate FVB/N WT and Tg[CX1-eGFP-Kir6.1AAA] controls (Figure 3C). This aggravated energy use was accompanied by relatively lower body weight and adipocyte area in Tg[MyoD-Kir6.1AAA] compared to WT or Tg[CX1-eGFP-Kir6.1AAA] littermates (Figure 3D–3F).

The contribution of K_{ATP} channels to myocardial energy consumption was assessed in hearts isolated from Kir6.2-KO under workloads set by pacing within the physiological range of 460–670 beats/min. Hearts lacking K_{ATP} channels exhibited augmented oxygen consumption, indicating an elevated energy cost of cardiac performance compared to WT (Figure 4A). At imposed workloads, progressive reduction of myocardial action potential duration (APD_{90}), characteristic for WT, was absent in Kir6.2-KO hearts as assessed from monophasic action potential recordings (Figure 4B). In WT hearts, workload-induced shortening of action potentials was reversed by the K_{ATP} channel blocker glyburide (10μM) underscoring the contribution of K_{ATP} channels in modulating myocardial excitability across the range of physiological cardiac rates. Absence of K_{ATP} channel function augmented cardiac mechanical work, measured as an integrated left ventricular pressure per cardiac cycle (Figure 4C), and induced overexpression of Na^+/K^+ pumps (Figure 4D and 4E), identifying these and myosin ATPase as molecular contributors to increased energy use.

Heightened muscle performance requires mobilization of bodily energy stores (Ghanassia et al., 2007). Analysis of telemetry-recorded heart rates revealed a two-peak distribution in the 400 to 800 beats/min range for WT and Kir6.2-KO during continuous daily activity (Figure 4F). This profile reflected normally-distributed heart rate variability that characterizes low *versus* high activity periods in each cohort. Fitting these distributions with the sum of two Gaussian functions indicated that while the highest mean heart rate was equivalent for Kir6.2-KO and WT (674 *versus* 670 beats/min, respectively), the lower characteristic mean value in Kir6.2-KO (570 beats/min) was right-shifted relative to WT (536 beats/min). The absence of K_{ATP} channels thereby provoked a partial redistribution of heart rate events from the region of 500 beats/min to that of 600 beats/min (Figure 4F). Thus, even in periods of low activity, Kir6.2-KO hearts are prompted to perform at rates higher than the WT, a feature characteristic of a hypermetabolic state (Bachman et al., 2004) characterized by augmented demand for oxygen and substrate delivery. In fact, the increased EE in Kir6.2-KO striated muscles intensified the mobilization of glycogen and fat energy depots, reducing muscular and hepatic glycogen stores within 16 h of fasting compared to WT (Figure 5A and 5B). This glycogen change in Kir6.2-KO is in line with increased muscle glucose uptake (Miki et al., 2002), augmented insulin sensitivity and a prominent drop of blood glucose levels under fasting and after exhaustion (Figure S1 and S2). Further, increased lipolysis in Kir6.2-KO revealed by fasting or in post-exercise recovery (Figure S1) caused a reduction of adipocyte size compared to WT (Figure 5C). Thus, lack of K_{ATP} channel function that precipitated inefficient EE in skeletal and cardiac muscles compromised bodily energy stores.

Inefficient energetics in K_{ATP} channel knockout fails to support intense workload

Endurance, or the ability to withstand activity-related workload, relies on the efficiency of body energetics. Maximal oxygen consumption ($\dot{V}O_{2max}$) reflects the maximal rate of energy production and the ability of the cardiovascular system to support physical performance at highest workloads by ensuring oxygen delivery to skeletal muscle (Joyner, 1991). Here, under treadmill testing, WT and Kir6.2-KO achieved similar $\dot{V}O_{2max}$, 7817±364 ml/kg/h (n=7) *versus* 8311±253 ml/kg/h (n=9) respectively, indicating equivalent oxidative phosphorylation potentials. Although $\dot{V}O_{2max}$ sets the upper limit for energy production, it does not determine ultimate performance (Zoll et al., 2002). Indeed, despite similar energy consumption rates at $\dot{V}O_{2max}$, i.e., 38.6±0.9 cal/g/h and 37.4±0.9 cal/g/h, K_{ATP} channel knockouts attained a total

work of 17.9±3.2 Joules (20 m/min at 15° inclination; n=8) below the 27.0±2.8 Joules (22.5 m/min at 20° inclination; n=9; $p<0.05$) achieved by more energy-efficient WT counterparts.

The efficiencies of the cardiovascular system and body energy resource recruitment were assessed in response to maximal workload (Barbato et al., 1998). Calorimetry-derived data normalized as $R(t)=(\dot{V}O_2 - \dot{V}O_{2min}) / (\dot{V}O_{2max} - \dot{V}O_{2min})$, where the oxygen consumption rate ($\dot{V}O_2$) was accelerated from $\dot{V}O_{2min}$ (at 2 mW) to $\dot{V}O_{2max}$ (at 30 mW workload), were fitted by the Gompertz function, $R(t)=\exp[-\exp(-(t-t_{max})/t_r)]$ where $1/t_r$ is the maximum growth rate at time t_{max} (Figure 6A). Both parameters were significantly slower for Kir6.2-KO (t_r=68±3.4 s and t_{max}=204±5.6 s, n=11) compared to WT (t_r=56±3.0 s and t_{max}=187±3.5 s, n=10; $p<0.05$). Oxygen deficit at the onset of exercise, calculated as the area above corresponding Gompertz curves, was higher for Kir6.2-KO (242.2±7.2 s, n=11) compared to WT (220.1±5.2 s, n=10; ANOVA $p<0.05$; Figure 6A). The increased oxygen deficit in Kir6.2-KO was accompanied by reversed substrate utilization dynamics compared to WT. On exercise initiation, mice lacking K_{ATP} channels demonstrated deficit of carbohydrate and raised lipid oxidation (Figure 2H and Figure 6A). These trends were reversed upon approaching $\dot{V}O_{2max}$ and exhaustion (Figure 6A), when Kir6.2-KO exhibited an energetically less efficient combination of increased carbohydrate and depressed lipid oxidation. Impaired mobilization of aerobic systems in Kir6.2-KO was linked to stimulation of anaerobic metabolic pathways manifested by development of lactic acidosis (Figure 6B). At exercise termination due to exhaustion, precipitous drop of oxygen consumption, fast decline of carbohydrate and lipid oxidation (Figure 6A), bradycardia and reduced mobility (Figure S3) collectively indicated that the circulatory system of Kir6.2-KO was unable to sustain substrate and oxygen supply. In fact, in response to stimulation with the sympathomimetic isoproterenol (10 μM), Kir6.2-KO hearts were unable to maintain performance for as long as WT hearts (Figure 6C).

Under voluntary activity, Kir6.2-KO also exhibited a low overall performance capacity compared to WT (Figure 6D). In contrast to coerced workload imposed by a treadmill regimen, free-access running wheels allow measurement of stress-free exercise capacity (Momken et al., 2005). Patterns of voluntary wheel runs were collected throughout 24-h intervals (Figure 6D), and bursts of activity, i.e., continuous periods of wheel rotations, accumulated in time-event distributions reflecting individual voluntary activity patterns (Figure 6E). Analysis of distributions revealed a similar total number of exercise attempts for both cohorts, yet a halved mean time of activity intervals for Kir6.2-KO compared to WT (Figure 6F). The superior ability of WT to sustain voluntary performance was further highlighted by a running distance that exceeded that of Kir6.2-KO counterparts (Figure 6F). Thus, lack of K_{ATP} channels impaired voluntary exercise, suggesting a critical role for these biosensors in optimizing activity-related energy use.

Kir6.2-KO are resistant to high-fat diet induced obesity

As disruption of K_{ATP} channel function raised the energy cost of exercise and non-exercise activity, resistance to diet-induced obesity was assessed. WT and Kir6.2-KO were challenged with a Western-type high-fat diet, starting at 11 weeks of age for 160 days of prospective monitoring (Figure 7A). Under continuous high-fat diet regimen, WT progressively acquired an obese phenotype in contrast to Kir6.2-KO that demonstrated obesity-resistance despite comparable food intake (Figure 7A and 7B). Throughout follow-up, Kir6.2-KO displayed lower body weight and rate of body weight gain than age-matched WT. High-fat diet compared to regular chow diet doubled the rate of weight gain in WT, i.e., 0.138 g/day (r^2=0.96, n=10) *versus* 0.071 g/day (r^2=0.87, n=10), respectively (Figure 7C). In Kir6.2-KO the rate of body weight gain was increased from 0.027 g/day under regular diet (r^2=0.95, n=10) to 0.074 g/day under high-fat diet (r^2=0.96, n=10) resulting in a body weight of Kir6.2-KO under high-fat

diet that did not exceed that of WT under regular diet (Figure 7C). Thus, the anti-obesity effect evoked by K_{ATP} channel dysfunction was preserved under high-fat diet challenge.

DISCUSSION

Sarcolemmal K_{ATP} channels are recognized molecular metabolic sensors that modulate membrane excitability according to cellular energy availability, yet their actual homeostatic role remains partially understood. Metabolic sensing by K_{ATP} channels has been typically assigned to a protective response under severe energy insult, such as acute ischemia, sympathetic distress or muscle fatigue (Matar et al., 2000; Zingman et al., 2002; Renaud 2002; Gumina et al., 2003; Miki and Seino, 2005; Yamada et al, 2006; Cifelli et al., 2007; Reyes et al., 2007). This study establishes a previously unrecognized role for sarcolemmal K_{ATP} channels in the continuous regulation of cellular energy use under non-stressed, physiological states. In this way, K_{ATP} channels emerge as important components of a cellular energy-sparing system that optimizes muscle energy expenditure. Lack of this K_{ATP} channel-dependent energy-controlling mechanism exaggerated energy use by heart and skeletal muscle, dissipating bodily glycogen/fat depots and promoting lower weight. The observed resistance to body weight gain under a high-fat diet, induced by K_{ATP} channel-deficiency, provides a basis for potential anti-obesity treatment (Watt et al., 2006). The sarcolemmal K_{ATP} channel, suitable for manipulation to render skeletal muscle increasingly thermogenic at rest and less fuel efficient in exercise (Himms-Hagen, 2004), thus represents a molecular target to magnify the benefit of activity for obesity treatment or prevention.

The energy-controlling function of K_{ATP} channels is based on the unique ability to feedback bioenergetic cues into constraints on cellular energy expenses for myofibrillar contraction and re-sequestration of Ca^{2+} and Na^{+} ions by opposing myocyte depolarization (Nichols and Lederer, 1991; Gong et al., 2000; Zingman et al., 2002; Thabet et al., 2005; Cifelli et al., 2007, 2008). By virtue of sensing even minor changes in cellular nucleotide content (Abraham et al., 2002; Selivanov et al., 2004), K_{ATP} channels could decode cellular metabolic dynamics during regular daily activity. Indeed, K_{ATP} channel-driven shortening of action potentials demonstrated here, within the physiological range of cardiac rates, ensured reduced oxygen consumption. An overload of ATPases supporting ion homeostasis was exposed by Na^{+}/K^{+} pump upregulation precipitated in the absence of sarcolemmal K_{ATP} channel function. Escalation of fuel metabolism in striated muscles translated to whole-body energy overuse in both Kir6.2-KO and Tg[MyoD-Kir6.1AAA] K_{ATP} channel-deficient models, manifested by reduction in fat depots and limited weight gain.

Characteristic of hypermetabolic states (Bachman et al., 2004), the increased energy demand in the absence of K_{ATP} channels entailed acceleration of cardiac rate, initiating a “vicious” cycle in which magnified cardiac mechanical work imposed further energy use and mobilization of glycogen and fat stores. Yet, while unchallenged, Kir6.2-KO did not exhibit a deficit in caloric intake or blood energy substrates despite the role of K_{ATP} channels in glucose homeostasis (Miki et al., 1998; Aguilar-Bryan et al., 2001; Ashcroft, 2005) and possibly in appetite control (Spanswick et al., 1997). The accelerated metabolism profile of Kir6.2-KO resembles transgenic models overexpressing mitochondria uncoupling proteins in skeletal muscle (UCP-TG; Li et al., 2000). Although sharing with UCP-TG properties of a lean phenotype, enhanced insulin sensitivity and glucose uptake (Li et al., 2000; Miki et al., 2002; Minami et al., 2003), Kir6.2-KO, by reaching $\dot{V}O_{2max}$ equivalent to WT, exhibited an unaltered oxidative phosphorylation capacity (Mootha et al., 1997) and sarcoplasmic nucleotide levels (Zingman et al., 2002). Thus, enhanced mobilization of body energy depots in Kir6.2-KO, while maintaining phosphocreatine and nucleotide pools, limits body weight gain.

Inefficient energy control in the absence of K_{ATP} channels endowed resistance to diet-induced obesity, although at the cost of decreased workload endurance. In fact, the oxygen deficit identified in Kir6.2-KO at workload initiation indicated delayed activation of enzymatic reactions and substrate mobilization required for skeletal muscle oxidative metabolism (McArdle, 1996). This was counterbalanced by anaerobic processes that, although compensating for energy deficit, provoked excessive lactate accumulation. The developed lactic acidosis suppressed lipolysis at peak exercise (Liu et al., 2009), and further compromised cardiac function critical in maintaining physical activity (Nielsen et al., 2002; Zingman et al., 2002; Kane et al., 2004). Accordingly, the Kir6.2-KO was unable to sustain stress-free voluntary performance despite an equal-with-WT number of exercise attempts.

In summary, this study demonstrates that sarcolemmal K_{ATP} channels not only respond to metabolic stress but continuously control energy use by cardiac and skeletal muscles, thereby promoting body energy conservation. Positive energy balance favoring obesity would be therefore moderated by tissue-specific interruption of K_{ATP} channel-driven optimization of energy use, offering a paradigm in weight control.

Experimental Procedures

Animal models

K_{ATP} channel-deficient mice were generated by targeted disruption of the *KCNJ11* gene (Miki et al., 1998). Due to the proximity of the mutated gene with the gene encoding albino hair color in SV129 embryonic stem cells used to create the knockout, Kir6.2-knockout (Kir6.2-KO) mice remained white upon backbreeding into the black C57BL/6 line (WT) for 10 generations. Experiments were performed with male mice, 3–4 months of age preceding divergence in body weight and fat distribution, unless otherwise indicated. Transgenic Tg[CX1-eGFP-Kir6.1-AAA] mice were obtained from the FVB/N mouse strain using a non-conducting Kir6.1AAA pore mutant where a Gly-Phe-Gly motif critical for K^+ permeation was replaced by Ala-Ala-Ala (Malester et al., 2007). Kir6.1AAA was subcloned downstream of the *loxP* sites flanking eGFP coding region and a stop codon, in such a way that dominant negative suppression of Kir6.2/SUR2A could be initiated by expression of Cre recombinase. Accordingly, skeletal muscle-specific ablation of K_{ATP} channel activity was achieved by crossing Tg[CX1-eGFP-Kir6.1-AAA] and MyoD-cre transgenic mice that express Cre recombinase under control of the MyoD promoter (Chen et al., 2005). Protocols were approved by Mayo Clinic and University of Iowa Institutional Animal Care and Use Committees.

Animal maintenance and diets

Mice were maintained in a temperature-controlled (25°C) facility on a 12-h light/dark cycle and fed with regular chow diet (PicoLab® Rodent Diet 20 5053; PMI Nutrition International, St Louis, MO) containing 5% fat accounting for ~13% of caloric content. A subset of animals was fed a high-fat diet containing 9% fat (~22% of the diet's caloric content; PicoLab® Mouse Diet 20 5058). Food intake was measured using a food consumption monitoring system (Columbus Instruments; Columbus, OH).

Magnetic resonance imaging

Transverse sections at the T3–T7 and L1–L5 levels were obtained under isoflurane anesthesia using a 7 Tesla scanner (Bruker; Billerica, MA) by a spin-echo method (Yamada et al., 2006). Analyze (Mayo Foundation; Rochester, MN) and MetaMorph (Molecular Devices; Sunnyvale, CA) softwares were used for image analysis.

Histochemistry

Liver and skeletal muscle samples were harvested from 16-h fasting animals, flash-frozen in isopentane/liquid nitrogen, and Periodic Acid Schiff (PAS) used for staining of glycogen content. Gluteal subcutaneous white fat was fixed in 10% buffered formalin, and stained with hematoxylin-eosin (Kane et al., 2004). Micrographs were taken by a KS-4000 Axiocam digital camera with an Axioplan 2 light microscope (Carl Zeiss MicroImaging, Thornwood, NY) and analyzed using MetaMorph.

Glycogen biochemical assay

Hepatic tissue and *gastrocnemius* muscles were harvested from fasting animals, homogenized in chilled 0.03 N HCl, sonicated for 45 s using a Branson Sonifier 450 (Branson, Danbury, CT), and boiled for 5 min. Samples were separated for measurement of free glucose or boiled in 2 N HCl for 3 h to hydrolyze glycogen content. Samples were then centrifuged for 1 min at 13,000 rpm and hydrolysis stopped by alkalization. Glucose levels were measured using a Glucose Assay Kit (Biovision Inc, Mountain View, CA), and free glucose concentration subtracted from glycogen-produced glucose. Results were normalized to wet tissue weights.

Analytical procedures

Blood lactate and pH were determined using a 5700 Gem-Primier3000 Gas/Electrolyte analyzer (Instrumentation Laboratory; Lexington, MA).

Locomotor activity

Activity was monitored using implanted telemetric devices (Data Science International; St. Paul, MN). Variations in signal strength due to change in animal orientation or distance from the receiver were averaged for each 10 s periods, and counted as movements per min (min^{-1}) revealing the level of activity. All activity levels were collected into histograms with 6 min^{-1} bin width implying that a certain activity level a_i was achieved with attaining all preceding activity levels, i.e., all bins from a_1 to a_i were incremented by 10 s. Mean activity level, a_0, was obtained by fitting each histogram with a single exponential function, $T=T_0 \cdot \exp(-k/a_0)$, where T_0 denotes total time of activity (the first histogram bin); and k, the activity level variable.

Indirect calorimetry and treadmill exercise

Indirect calorimetry was performed using metabolic chambers (Oxymax, Columbus Instruments). Experiments were synchronized with a start-time of 19:00 h, for continuous monitoring under *ad libitum* chow diet. EE was determined based on rate of oxygen consumption ($\dot{V}O_2$) and carbon dioxide production ($\dot{V}CO_2$):

$$EE=3.815\dot{V}O_2+1.232\dot{V}CO_2.$$

The calorimeter was calibrated before each measurement with a standard span gas (0.501% CO_2, 20.53% O_2 balanced with N_2), and cross-calibrated against room air at every fifth measurement. Maximal rates of oxygen consumption ($\dot{V}O_{2max}$) and EE during physical activity were measured using a modular treadmill connected to the calorimetry system. Ten days before exercise tests, mice were acclimated daily for a nonmoving treadmill followed by 15 min at a velocity of 3.5 m/min. The treadmill velocity, set for a constant workload rate (W), was adjusted to body weight for each animal as $W/(m\ g)/\sin(\alpha)$, where m is body weight; g, acceleration due to gravity (9.8 m/s^2);α, treadmill inclination. The exercise-endurance protocol was performed as described (Zingman et al, 2002). Differences in the rate of carbohydrate and lipid

consumption between cohorts were calculated based on $\dot{V}O_2$ and 2 $\dot{V}CO_2$ values using Ferrannini's equations (Ferrannini, 1988):

$$\text{Carbohydrates}(g/min) = 4.55\dot{V}CO_2(L/min) - 3.21\dot{V}O_2(L/min) - 2.87N(mg/min)$$

$$\text{Lipids oxydation}\ (g/min) = 1.67(\dot{V}O_2 - \dot{V}CO_2)(L/min) - 1.92N(mg/min),$$

where N is the rate of urinary nitrogen excretion used to estimate protein oxidation, with the assumption that urinary nitrogen is equivalent in experimental groups. Errors for the difference in substrate utilization between Kir6.2-KO and WT mean values were calculated using the quadrature rule according to the propagation of uncertainties for normally distributed independent measures (Tayler, 1997).

Patch-clamp recordings

Skeletal muscle cells from *musculus flexor digiti brevis* were enzymatically isolated (Lueck et al., 2007), and single channel currents were recorded in the cell-attached mode of the patch-clamp technique at a holding command potential of +60 mV set in a pipette electrode using an Axopatch 200B amplifier (Molecular Devices; Sunnyvale, CA). Patch pipettes, filled with a solution containing (in mM): KCl 140, $CaCl_2$ 1, $MgCl_2$ 1, HEPES-KOH 5 (pH 7.3), had a resistance of 5–7 MΩ. Cells were bathed in (in mM): KCl 140, $MgCl_2$ 1, EGTA 5, HEPES-KOH 5 (pH 7.3). Measurements were performed at 30°C.

Western blotting

Protein extracts were prepared by homogenizing ventricular tissue in NaCl 150 mM, Tris-HCl 50 mM, pH 7.8 supplemented with 1% Triton X-100 and protease inhibitors. Electrophoresis was performed on 3–8% gradient Nu-Page Tris-Acetate gel and transferred to polyvinylidene difluoride membranes (InVitrogen). Mouse monoclonal antibodies against Na^+/K^+ ATPase (Afinity Bioreagents, Rockford, IL) and anti-mouse HP-conjugated secondary antibody (Santa Cruz Biotechnology, Inc. Sant-Cruz, CA) were used.

Monophasic action potential (MAP), left ventricular (LV) pressure and oxygen consumption

Isolated hearts were retrogradely perfused at 90 mmHg with Krebs–Henseleit buffer bubbled with 95% O_2/5% CO_2 (37°C, pH 7.4). Hearts were paced (A310 Accupulser; World Precision Instruments; Sarasota, FL) using a catheter positioned in the right ventricular apex (NuMed; Hopkinton, NY). A MAP probe (EP Technologies; Sunnyvale, CA) was maintained at the LV epicardium, and amplified signals (IsoDam; World Precision Instruments; Sarasota, FL) were acquired at 11.8 kHz (Zingman et al., 2002). MAPs were analyzed at 90% of repolarization (APD_{90}). LV pressure was measured using a fluid-filled balloon attached to a pressure transducer (Harvard Apparatus; Holliston, MA), and diastolic pressure was set to 10 mmHg. Oxygen consumption was calculated based on Henry's Law as the difference between the oxygen partial tension measured, using the 5700 GemPrimier3000 Gas/Electrolyte analyzer, in the perfusate prior (PO_{2cntr}) and after (PO_2) heart passage. The rate of oxygen consumption ($\dot{V}O_2$)was calculated as:

$$\dot{V}O_2=(PO_{2cntr} - PO_2) \cdot \alpha \cdot \nu/m_h,$$

where ν is rate of coronary flow measured by a T106 flow-meter (Transonic System Inc.; Ithaca, NY); α = (0.024 ml O_2 per ml H_2O)/760 mmHg denotes the Bunsen's solubility coefficient (Sinaasappel et al., 1999); and m_h is heart wet weight.

Voluntary performance

Mice were housed in individual cages with free access to attached running wheels of 242 mm diameter (Mini Mitter Co.; Bend, OR). Wheel turns were counted with a Mini Mitter Magnetic Switch, averaged for each 10 s, converted to RPM (rotations per minute) by a DSI acquisition system (Data Sciences International; St. Paul, MN). Exercise intervals (bursts of activity) were accumulated in Poisson time-event distributions with 10 s bin width implying that a running burst duration corresponding to n_i was associated with attainment of all preceding activity duration intervals, i.e. all bins from n_1 to n_i were incremented by a unit. Thus, the first bin consists of a total number of bursts (i.e. number of exercise attempts), and the probability of a running interval with duration *t* is proportional to $e^{-\alpha t}$, where 1/α is the mean time of activity burst duration. Running distance was calculated as $1/6\pi D \cdot \Sigma RMP_i$, where *D* is wheel diameter and ΣRMP_i is sum of averaged RPM values.

Statistical analysis

Results are expressed as mean±SEM. Student's *t*-test was used to define *p* values unless otherwise indicated. A *p* value of <0.05 was considered statistically significant.

Supplementary Material

Refer to Web version on PubMed Central for supplementary material.

Acknowledgments

The authors are particularly grateful to Dr. T. Miki (Chiba University) and Dr. S. Seino (Kobe University) for providing the Kir6.2-KO model. We further thank Drs. P. Mishra and S. Macura, Mayo Clinic Analytical NMR Facility, for expertise with NMR imaging, Drs. K. Campbell and J. Lueck (University of Iowa) for guidance with myofiber isolation, L. Rowe (Mayo Clinic) for assistance with histological specimens, E. Stepniak (University of Iowa) for technical assistance, and Dr. S.I. Loginov (Surgut University) for valuable discussion. This work was supported by Gerstner Family Career Development Award in Individualized Medicine (A.E.A.), Mayo Graduate School Fellowship (S.R.); American Society for Clinical Pharmacology and Therapeutics Young Investigator Award (S.Y.); NIH T32GM008685 (S.S.); NIH RO1HL64822 (A.T.); NIH AR052777 (D.J.G.), Marriott Heart Diseases Research Program, Marriott Foundation (A.T.); and in part by Medical Research Initiative Roy J. Carver Charitable Trust pilot grant and Fraternal Order of Eagles, Iowa Aerie grant (L.V.Z. and D.M.H-Z.).

References

Abraham MR, Selivanov VA, Hodgson D, Pucar D, Zingman LV, Wieringa B, Dzeja PP, Alekseev AE, Terzic A. Coupling of cell energetics with membrane metabolic sensing: Integrative signaling through creatine kinase phosphor-transfer disrupted by *M-CK* gene knockout. J. Biol. Chem 2002;277:24427–24434. [PubMed: 11967264]

Aguilar-Bryan L, Bryan J, Nakazaki M. Of mice and men: K_{ATP} channels and insulin secretion. Recent Prog. Horm. Res 2001;56:47–68. [PubMed: 11237225]

Alekseev AE, Hodgson DM, Karger AB, Park S, Zingman LV, Terzic A. ATP-sensitive K^+ channel channel/enzyme multimer: metabolic gating in the heart. J. Mol. Cell. Cardiol 2005;38:895–905. [PubMed: 15910874]

Ashcroft FM. ATP-sensitive potassium channelopathies: focus on insulin secretion. J. Clin. Invest 2005;115:2047–2058. [PubMed: 16075046]

Babenko AP, Aguilar-Bryan L, Bryan J. A view of SUR/KIR6.X, K_{ATP} channels. Annu. Rev. Physiol 1998;60:667–687. [PubMed: 9558481]

Barbato JC, Koch LG, Darvish A, Cicila GT, Metting PJ, Britton SL. Spectrum of aerobic endurance running performance in eleven inbred strains of rats. J. Appl. Physiol 1998;85:530–536. [PubMed: 9688730]

Bachman ES, Hampton TG, Dhillon H, Amende I, Wang J, Morgan JP, Hollenberg AN. Effect of hyperthyroidism on spontaneous physical activity and energy expenditure in rats. Endocrinology 2004;145:2767–2774. [PubMed: 15016719]

Carrasco A, Dzeja P, Alekseev A, Pucar D, Zingman L, Abraham M, Hodgson D, Bienengraeber M, Puceat M, Janssen E, et al. Adenylate kinase phosphotransfer communicates cellular energetic signals to ATP-sensitive potassium channels. Proc. Natl. Acad. Sci. USA 2001;98:7623–7628. [PubMed: 11390963]

Celi FS. Brown adipose tissue – when it pays to be inefficient. N. Engl. J. Med 2009;360:1553–1556. [PubMed: 19357412]

Chen JC, Mortimer J, Marley J, Goldhamer DJ. MyoD-cre transgenic mice: a model for conditional mutagenesis and lineage tracing of skeletal muscle. Genesis 2005;41:116–121. [PubMed: 15729689]

Cifelli C, Bourassa F, Gariépy L, Banas K, Maria Benkhalti M, Renaud J-M. K_{ATP} channel deficiency in mouse flexor digitorum brevis causes fibre damage and impairs Ca^{2+} release and force development during fatigue *in vitro*. J. Physiol 2007;582:843–857. [PubMed: 17510189]

Cifelli C, Boudreault L, Gong B, Bercier JP, Renaud J-M. Contractile dysfunctions in ATP-dependent K^+ channel-deficient mouse muscle during fatigue involve excessive depolarization and Ca^{2+} influx through L-type Ca^{2+} channels. Exp. Physiol 2008;93:1126–1138. [PubMed: 18586858]

Ferrannini E. The theoretical bases of indirect calorimetry: a review. Metabolism 1988;37:287–301. [PubMed: 3278194]

Ghanassia E, Brun J-F, Mercier J, Raynaud E. Oxidative mechanisms at rest and during exercise. Clinica Chimica Acta 2007;383:1–20.

Gong B, Miki T, Seino S, Renaud J-M. A K_{ATP} channel deficiency affects resting tension, not contractile force, during fatigue in skeletal muscle. Am. J. Physiol 2000;279:C1351–C1358.

Gumina RJ, Pucar D, Bast P, Hodgson DM, Kurtz CE, Dzeja PP, Miki T, Seino S, Terzic A. Knockout of Kir6.2 negates ischemic reconditioning-induced protection of myocardial energetics. Am. J. Physiol 2003;284:H2106–H2139.

Himms-Hagen J. Exercise in a pill: feasibility of energy expenditure targets. Curr. Drug Targets CNS Neurol. Disord 2004;3:389–409. [PubMed: 15544447]

Inagaki N, Gonoi T, Clement JP 4th, Namba N, Inazawa J, Gonzalez G, Aguilar-Bryan L, Seino S, Bryan J. Reconstitution of IK_{ATP}: an inward rectifier subunit plus the sulfonylurea receptor. Science 1995;270:1166–1170. [PubMed: 7502040]

Joyner MJ. Modeling: optimal marathon performance on the basis of physiological factors. J. Appl. Physiol 1991;70:683–687. [PubMed: 2022559]

Kane GC, Behfar A, Yamada S, Perez-Terzic C, O'Cochlain F, Reyes S, Dzeja PP, Miki T, Seino S, Terzic A. ATP-sensitive K^+ channel knockout compromises the metabolic benefit of exercise training, resulting in cardiac deficits. Diabetes 2004;53:S169–S175. [PubMed: 15561907]

Kunz WS. Control of oxidative phosphorylation in skeletal muscle. Biochim. Biophys. Acta 2001;1504:12–19. [PubMed: 11239481]

Levine JA, Eberhardt NL, Jensen MD. Role of nonexercise activity thermogenesis in resistance to fat gain in humans. Science 1999;283:212–214. [PubMed: 9880251]

Li B, Nolte LA, Ju J-S, Han DH, Coleman T, Holloszy JO, Semenkovich CF. Skeletal muscle respiratory uncoupling prevents diet-induced obesity and insulin resistance in mice. Nat. Med 2000;6:1115–1120. [PubMed: 11017142]

Liu C, Wu J, Zhu J, Kuei C, Yu J, Shelton J, Sutton SW, Li X, Yun SJ, Mirzadegan T, et al. Lactate inhibits lipolysis in fat cells through activation of an orphan G-protein-coupled receptor, GPR81. J. Biol. Chem 2009;284:2811–2822. [PubMed: 19047060]

Lueck JD, Lungu C, Mankodi A, Osborne RJ, Welle SL, Dirksen RT, Thornton CA. Chloride channelopathy in myotonic dystrophy resulting from loss of posttranscriptional regulation for CLCN1. Am. J. Physiol 2007;292:C1291–C1297.

Malester B, Tong X, Ghiu I, Kontogeorgis A, Gutstein DE, Xu J, Hendricks-Munoz KD, Coetzee WA. Transgenic expression of a dominant negative K_{ATP} channel subunit in the mouse endothelium: effects on coronary flow and endothelin-1 secretion. FASEB J 2007;21:2162–2172. [PubMed: 17341678]

Matar W, Nosek TM, Wong D, Renaud J-M. Pinacidil suppresses contractility and preserves energy but glibenclamide has no effect during muscle fatigue. Am. J. Physiol 2000;278:C404–C416.

McArdle, WD.; Katch, FI.; Katch, VL. Human energy expenditure during rest and physical activity. In: Balado, D., editor. In Exercise Physiology. 4th edition. Baltimore, MD: Williams & Wilkins; 1996. p. 151-164.

Miki T, Seino S. Roles of K_{ATP} channels as metabolic sensors in acute metabolic changes. J. Mol. Cell. Cardiol 2005;38:917–925. [PubMed: 15910876]

Miki T, Minami K, Zhang L, Morita M, Gonoi T, Shiuchi T, Minokoshi Y, Renaud J-M, Seino S. ATP-sensitive potassium channels participate in glucose uptake in skeletal muscle and adipose tissue. Am. J. Physiol 2002;283:E1178–E1184.

Miki T, Nagashima K, Tashiro F, Kotake K, Yoshitomi H, Tamamoto A, Gonoi T, Iwanaga T, Miyazaki J, Seino S. Defective insulin secretion and enhanced insulin action in K_{ATP} channel-deficient mice. Proc. Natl. Acad. Sci. USA 1998;95:10402–10406. [PubMed: 9724715]

Minami K, Morita M, Saraya A, Yano H, Terauchi Y, Miki T, Kuriyama T, Kadowaki T, Seino S. ATP-sensitive K^+ channel-mediated glucose uptake is independent of IRS-1/phosphatidylinositol 3-kinase signaling. Am. J. Physiol 2003;285:E1289–E1296.

Momken I, Lechêne P, Koulmann N, Fortin D, Mateo P, Doan BT, Hoerter J, Bigard X, Veksler V, Ventura-Clapier R. Impaired voluntary running capacity of creatine kinase-deficient mice. J. Physiol 2005;565:951–964. [PubMed: 15831533]

Mootha V, Arai AE, Balaban RS. Maximum oxidative phosphorylation capacity of the mammalian heart. Am. J. Physiol 1997;272:H769–H775. [PubMed: 9124437]

Nichols CG. K_{ATP} channels as molecular sensors of cellular metabolism. Nature 2006;440:470–476. [PubMed: 16554807]

Nichols CG, Lederer WJ. The regulation of ATP-sensitive K^+ channel activity in intact and permeabilized rat ventricular myocytes. J. Physiol 1990;423:91–110. [PubMed: 2388163]

Nichols CG, Lederer WJ. Adenosine triphosphate-sensitive potassium channels in the cardiovascular system. Am. J. Physiol 1991;261:H1675–H1686. [PubMed: 1750525]

Nichols CG, Shyng SL, Nestorowicz A, Glaser B, Clement JP, Gonzalez G, Aguilar-Bryan L, Permutt MA, Bryan J. Adenosine diphosphate as an intracellular regulator of insulin secretion. Science 1996;272:1785–1787. [PubMed: 8650576]

Nielsen HB, Bredmose PP, Str000F8;mstad M, Volianitis S, Quistorff B, Secher NH. Bicarbonate attenuates arterial desaturation during maximal exercise in humans. J. Appl. Physiol 2002;93:724–731. [PubMed: 12133884]

Ogden CL, Carroll MD, Curtin LR, McDowell MA, Tabak CJ, Flegal KM. Prevalence of overweight and obesity in the United States, 1999–2004. JAMA 2006;295:1549–1555. [PubMed: 16595758]

Renaud JM. Modulation of force development by Na^+, K^+, Na^+/K^+ pump and K_{ATP} channel during muscular activity. Can. J. Appl. Physiol 2002;27:296–315. [PubMed: 12180319]

Reyes S, Kane GC, Miki T, Seino S, Terzic A. K_{ATP} channels confer survival advantage in cocaine overdose. Mol Psychiatry 2007;12:1060–1061. [PubMed: 18043710]

Schwartz MW, Woods SC, Seeley RJ, Barash GS, Baskin DG, Leibel RL. Is the energy homeostasis system inherently biased toward weight gain? Diabetes 2003;52:232–238. [PubMed: 12540591]

Selivanov VA, Alekseev AE, Hodgson DM, Dzeja PP, Terzic A. Nucleotide-gated K_{ATP} channels integrated with creatine and adenylate kinases: amplification, tuning and sensing of energetic signals in the compartmentalized cellular environment. Mol. Cell. Biochem 2004:256–257. 243–256.

Sinaasappel M, Donkersloot C, Van Bommel J, Ince C. PO_2 measurements in the rat intestinal microcirculation. Am. J. Physiol 1999;39:G1515–G1520. [PubMed: 10362656]

Spanswick D, Smith MA, Groppi VE, Logan SD, Ashford MLJ. Leptin inhibits hypothalamic neurons by activation of ATP-sensitive potassium channels. Nature 1997;390:521–525. [PubMed: 9394003]

Tayler, JR. An Introduction to Error Analysis: the Study of Uncertainties in Physical Measurements. 2nd ed.. Sausalito, California: University Science Book; 1997.

Thabet M, Miki T, Seino S, Renaud J-M. Treadmill running causes significant fiber damage in skeletal muscle of K_{ATP} channel-deficient mice. Physiol. Genomics 2005;22:204–212. [PubMed: 15914579]

Watt MJ, Dzamko N, Thomas WG, Rose-John S, Ernst M, Carling D, Kemp BE, Febbraio MA, Steinberg GR. CNTF reverses obesity-induced insulin resistance by activating skeletal muscle AMPK. Nat. Med 2006;12:541–548. [PubMed: 16604088]

Weiss JN, Lamp ST. Cardiac ATP-sensitive K^+ channels. Evidence for preferential regulation by glycolysis. J. Gen. Physiol 1989;94:911–935. [PubMed: 2512370]

Yamada M, Isomoto S, Matsumoto S, Kondo C, Shindo T, Horio Y, Kurachi Y. Sulphonylurea receptor 2B and Kir6.1 form a sulphonylurea-sensitive but ATP-insensitive K^+ channel. J. Physiol 1997;499:715–720. [PubMed: 9130167]

Yamada S, Kane GC, Behfar A, Liu XK, Dyer RB, Faustino RS, Miki T, Seino S, Terzic A. Protection conferred by myocardial ATP-sensitive K^+ channels in pressure overload-induced congestive heart failure revealed in *KCNJ11* Kir6.2-null mutant. J. Physiol 2006;577:1053–1065. [PubMed: 17038430]

Zingman L, Hodgson D, Bast P, Kane G, Perez-Terzic C, Gumina R, Pucar D, Bienengraeber M, Miki T, Seino S, et al. A. Kir6.2 required for adaptation to stress. Proc. Natl. Acad. Sci. USA 2002;99:13278–13283. [PubMed: 12271142]

Zingman LV, Hodgson DM, Alekseev AE, Terzic A. Stress without distress: homeostatic role for K_{ATP} channels. Mol. Psychiatry 2003;8:253–254. [PubMed: 12660794]

Zoll J, Sanchez H, N'Guessan B, Ribera F, Lampert E, Bigard X, Serrurier B, Fortin D, Geny B, Veksler V, et al. Physical activity changes the regulation of mitochondrial respiration in human skeletal muscle. J. Physiol 2002;543:191–200. [PubMed: 12181291]

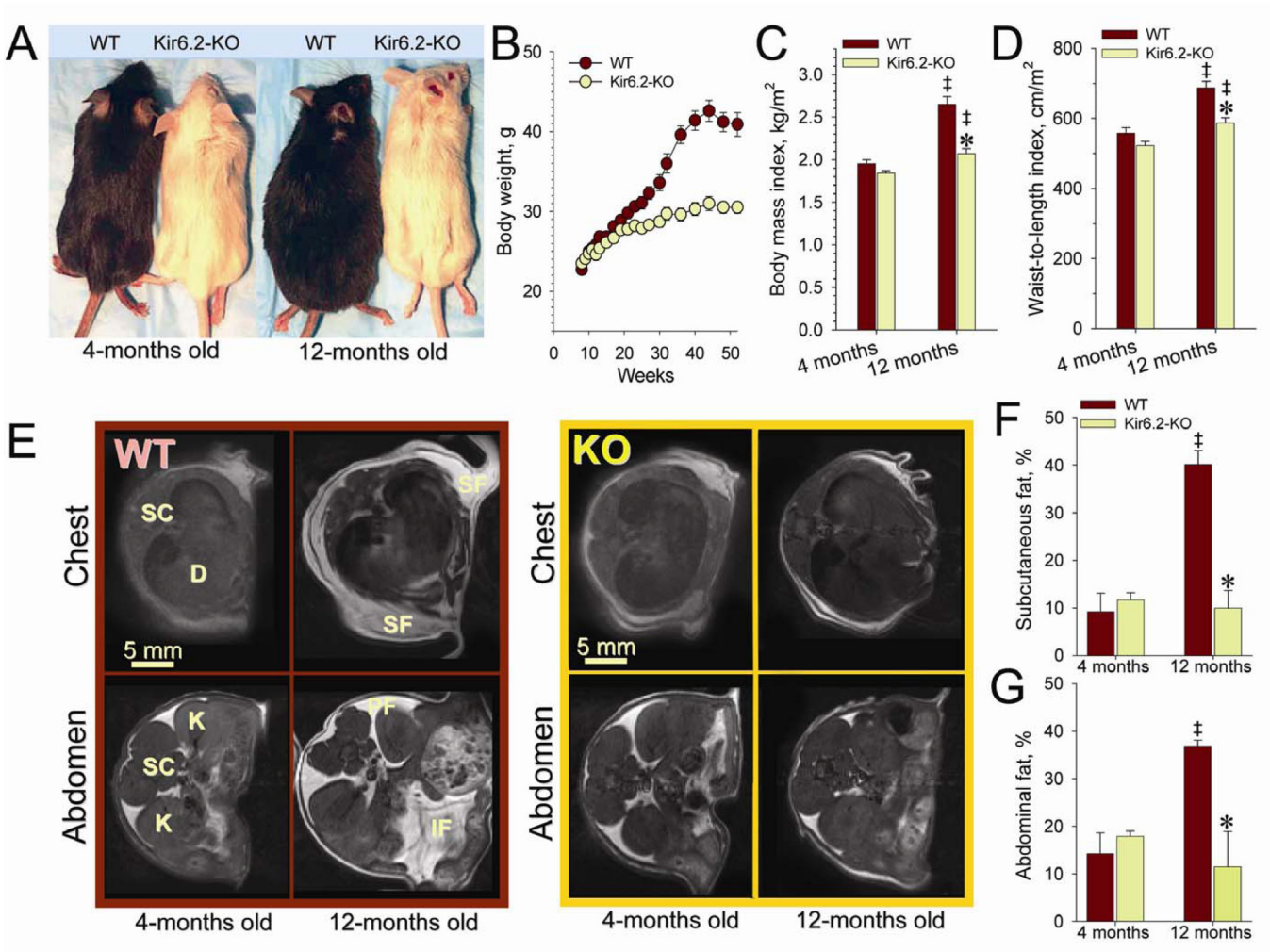

Figure 1. Kir6.2-KO mice inherit low body weight

(A) WT display larger trunk size compared to Kir6.2-KO at 1-year follow up.

(B) Divergence in body weight in individually caged WT (n=10) and Kir6.2-KO (n=10) by 5 months of age.

(C and D) Body mass index (BMI) calculated as the ratio of body weight to the square of body nasal-to-anal length, and waist-to-length index (WLI) calculated as the ratio of abdomen diameter to the square of body nasal-to-anal length, increased during maturation of WT and Kir6.2-KO (‡, $p<0.05$ at 12 *versus* 4-months within each cohort; n=10 in each group), with BMI and WLI significantly lower at 12 months in Kir6.2-KO compared to WT (*, $p<0.05$; n=10 in each group).

(E) Transverse MRI scans through thorax and abdomen of WT (left) and Kir6.2-KO (right) at 4 and 12 months. Abbreviations: D, diaphragm; IF, interstitial fat; K, kidney; PF, retroperitoneal fat; SC, spinal cord; SF, subcutaneous fat. Note prominent fat deposition in WT compared to Kir6.2-KO at 1-year of age.

(F and G) Mean areas of subcutaneous and abdominal fat, expressed relative to total cross-sectional area, were significantly increased in 12-months old WT compared to either 4-month-old WT (‡, $p<0.05$; n=4) or 12-month-old Kir6.2-KO (*, $p<0.05$; n=4). In contrast to WT, fat stores in Kir6.2-KO were statistically indistinguishable at both ages.

Data are mean±SEM.

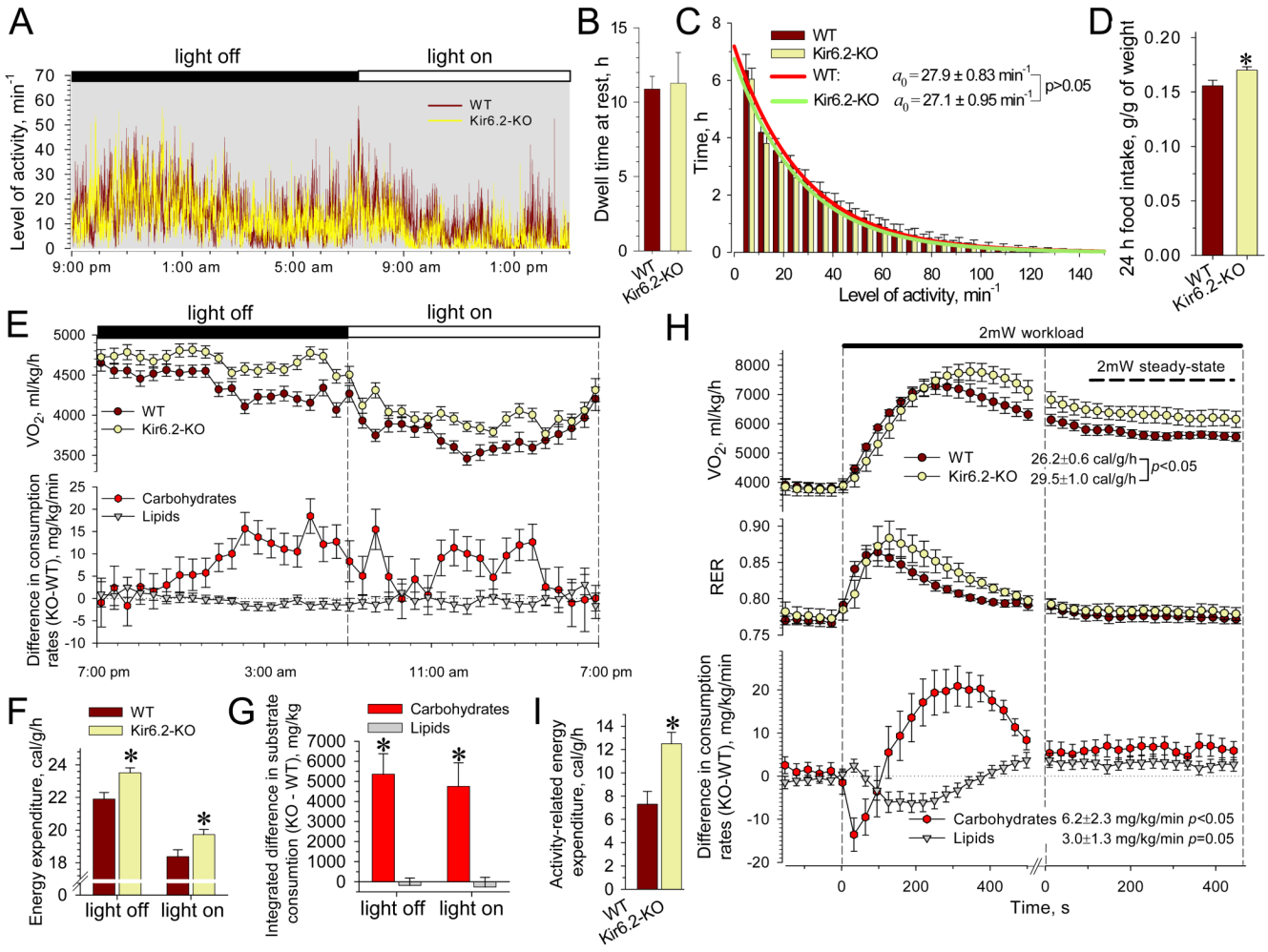

Figure 2. Activity, food intake and EE in WT and Kir6.2-KO

(A) Records of continuous locomotive activity monitored using implanted transmitting devices.

(B and C) Dwell time spent without movement was indistinguishable between WT and Kir6.2-KO (n=8 for each group). Fitting of the activity distributions, solid curves, revealed mean characteristic activities indistinguishable between WT and Kir6.2-KO.

(D) Food intake with regular chow diet, accumulated over 24 h and corrected for body weight, was higher in Kir6.2-KO (n=14) *versus* WT (n=16).

(E) Average time-course of oxygen consumption rates ($\dot{V}O_2$), and difference of substrate consumption rate calculated for Kir6.2-KO (n=19) relative to WT (n=17). Data points represent the average of 3 measurements from each animal.

(F) EE calculated based on $\dot{V}O_2$ and $\dot{V}CO_2$ values and averaged separately for light-on and light-off periods was higher in Kir6.2-KO *versus* WT.

(G) Cumulative substrate utilization obtained by integration over light-on and light-off periods revealed elevated carbohydrate consumption in Kir6.-KO compared to WT. Lipid utilization remained equivalent.

(H) $\dot{V}O_2$, respiratory exchange ratio (RER) and substrate consumption rates in WT (n=8) and Kir6.2-KO (n=8) were obtained within 30 s intervals during 2 mW treadmill test. At steady-state, Kir6.2-KO displayed an elevated EE compared to WT, accompanied with raised rates of substrate utilization.

(I) Activity-related EE was higher in Kir6.2-KO *versus* WT (n=8 in each group). Data are mean±SEM; *, $p<0.05$.

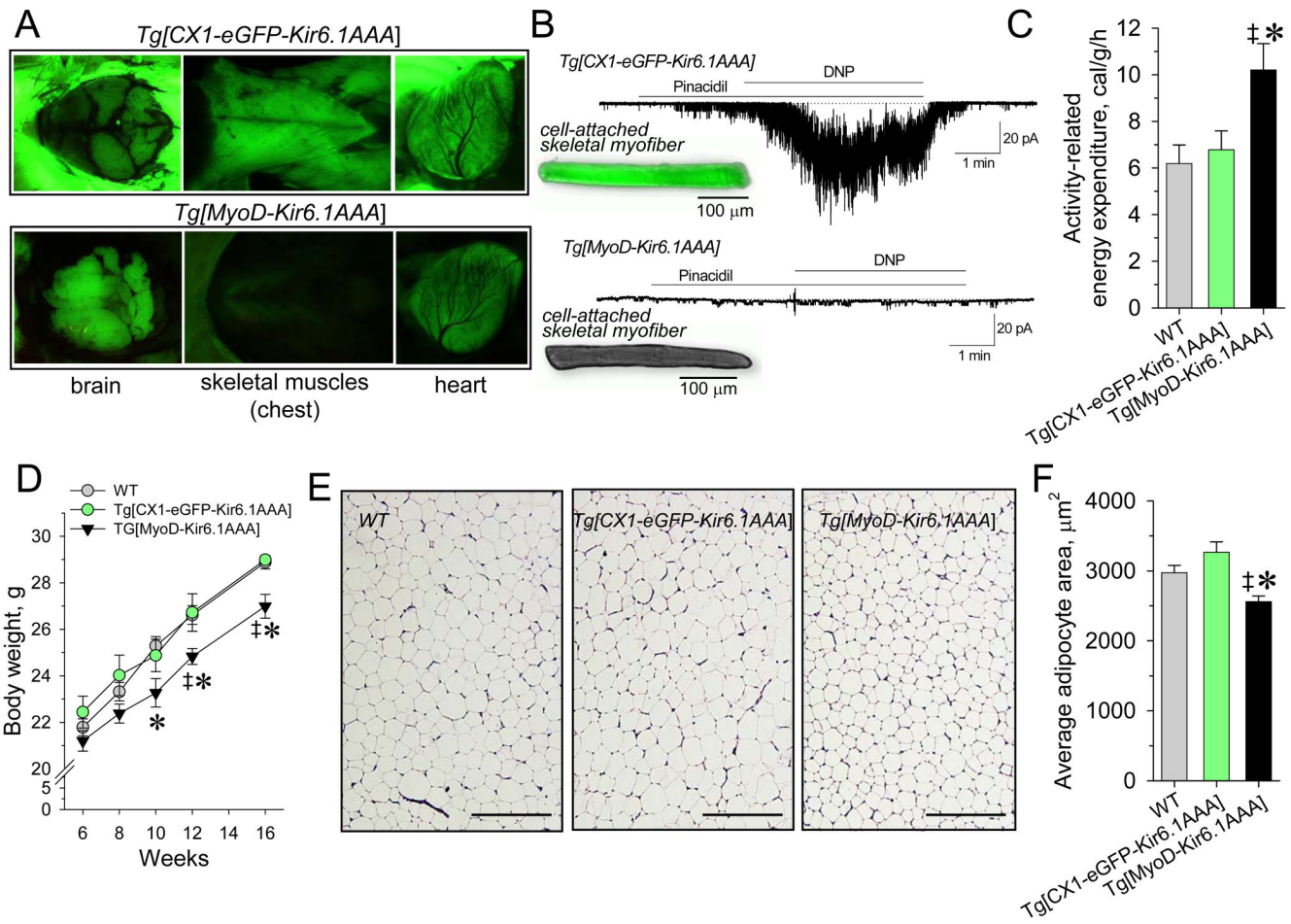

Figure 3. Elevated EE decreases body weight in Tg[MyoD-Kir6.1AAA]

(A) Brain and muscle tissues of Tg[CX1-eGFP-Kir6.1AAA] and Tg[MyoD-Kir6.1AAA] mice exposed to 525 nm wavelength light. Tg[MyoD-Kir6.1AAA], due to Cre-recombination of eGFP-coding region, lacked eGFP fluorescence exclusively in skeletal muscles.

(B) Expression of Kir6. 1AAA suppressed K_{ATP} channel function in skeletal muscle cells from Tg[MyoD-Kir6. 1AAA] as assessed by electrophysiology with no K_{ATP} channel response to pinacidil (50 μM) and 2,4-dinitrophenol (DNP, 200 μM), which induced vigorous K_{ATP} channel activation in Tg[CX1-eGFP-Kir6.1AAA] myofibers.

(C) Activity-related EE defined in 8 weeks old Tg[MyoD-Kir6.1AAA] (n=5) was significantly higher compared to FVB/N WT (‡, p<0.05; n=6) or Tg[CX1-eGFP-Kir6.1AAA] littermates (*, p<0.05; n=4).

(D) Body weight in Tg[MyoD-Kir6.1AAA] (n=6) was reduced compare to Tg[CX1-eGFP-Kir6.1AAA] (n=5;*, p<0.05) and FVB/N WT (n=8; ‡, p<0.05) littermates.

(E and F) Average cross-sectional area of individual adipocytes was reduced in Tg[MyoD-Kir6.1AAA] (n=3) compared to Tg[CX1-eGFP-Kir6.1AAA] (n=3;*, p<0.05) and FVB/N WT (n=3; ‡, p<0.05); scale bars, 200 μm.

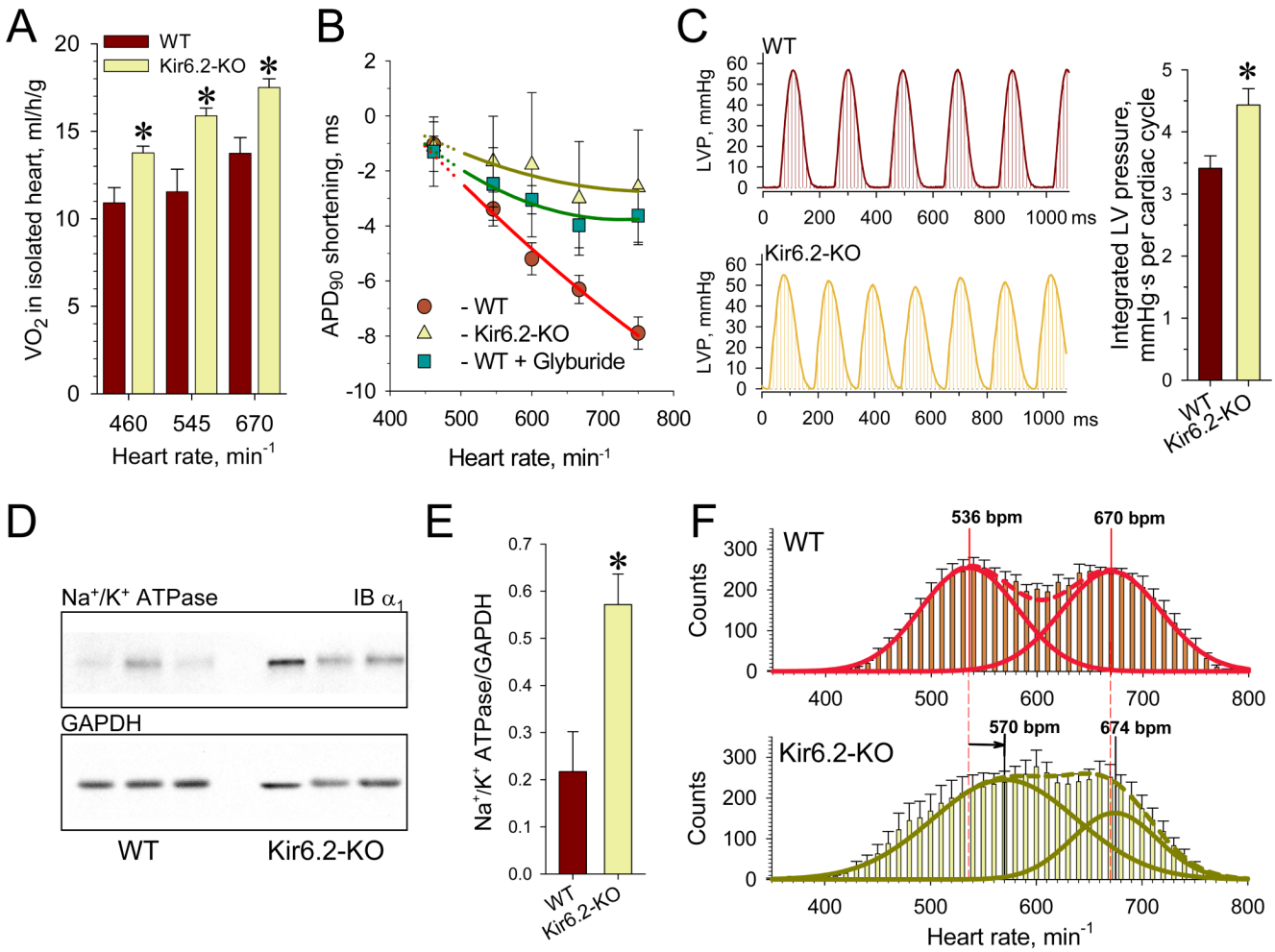

Figure 4. Increased EE and mechanical function of Kir6.2-KO isolated hearts

(A) Rate of oxygen consumption, measured in isolated perfused hearts revealed a significantly elevated energy demand in Kir6.2-KO *versus* WT (n=5 for each group).

(B) Pacing rates above 130 ms (460 beats/min) induced significant shortening of APD_{90} in WT (n=8) that was sensitive to the sulfonylurea glyburide (10 μM, n=4) but not in hearts from Kir6.2-KO (n=5). Solid lines were constructed as results of quadratic polynomial fitting of experimental data relative to APD_{90} at 150 ms pacing interval.

(C)Integrated left ventricular pressure was defined for 3–4 s long periods and divided by number of cardiac cycles in unpaced Kir6.2-KO and WT hearts (n=7 for each group).

(D and E) Overexpression of sarcolemmal Na^+/K^+ pumps in Kir6.2-KO compared to WT (n=3 for each group) revealed by Western blots.

(F) Histograms summarizing heart rates during 24-h long monitoring using telemetry in WT (n=11, top) and Kir6.2-KO (n=10, bottom). Dotted lines represent the fit of distributions with the sum of two Gaussian functions; solid lines indicate individual functions. Arrow indicates right shift of the lower mean heart rate in Kir6.2-KO relative to the corresponding value in WT.

Data are mean±SEM;*, $p<0.05$.

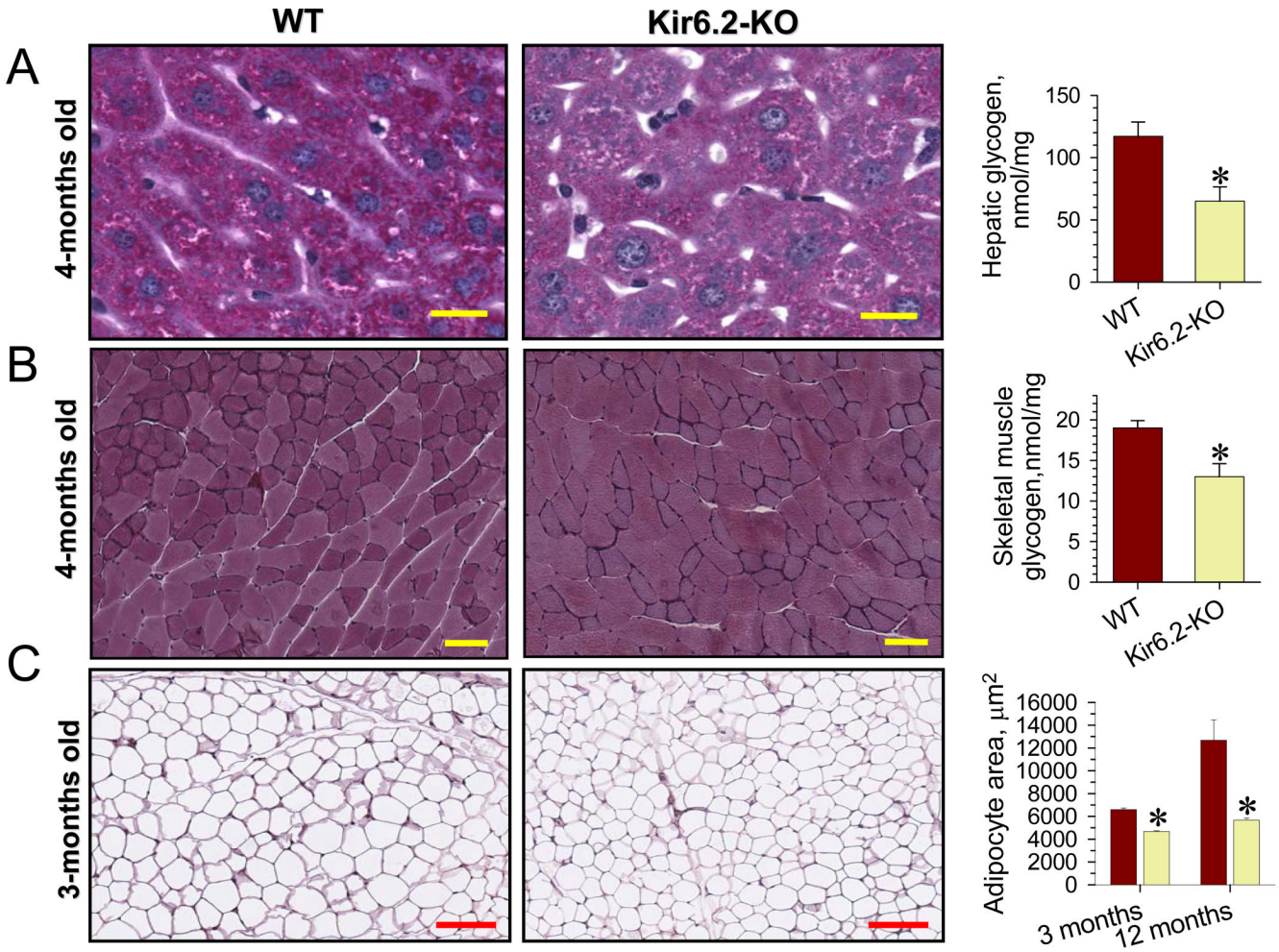

Figure 5. Reduced energy depots in Kir6.2-KO

(A) Left: PAS histology of hepatic tissue indicates depletion of glycogen stores in liver from Kir6.2-KO compared to WT. Scale bar; 100 µm (40x image magnification). Right: biochemical evaluation confirmed liver glycogen deficit in Kir6.2-KO compared to WT n=9 in each group).
(B) Left: PAS staining of skeletal muscle revealed significant depletion of glycogen in certain fibers from Kir6.2-KO *gastrocnemius* compared to WT. Scale bar: 200 µm (20x image magnification). Right: biochemical evaluation confirmed glycogen deficit in *gastrocnemius* from Kir6.2-KO (n=4) compared to WT (n=5).
(C) Left: Adipose tissue histology in WT and Kir6.2-KO (scale bars, 200 µm). Right: Average cross-sectional area of individual adipocytes was increased in WT compared to Kir6.2-KO by 3 months of age, and the difference progressed by 12 months (n=3 for each group).
Data are mean±SEM;*, $p<0.05$.

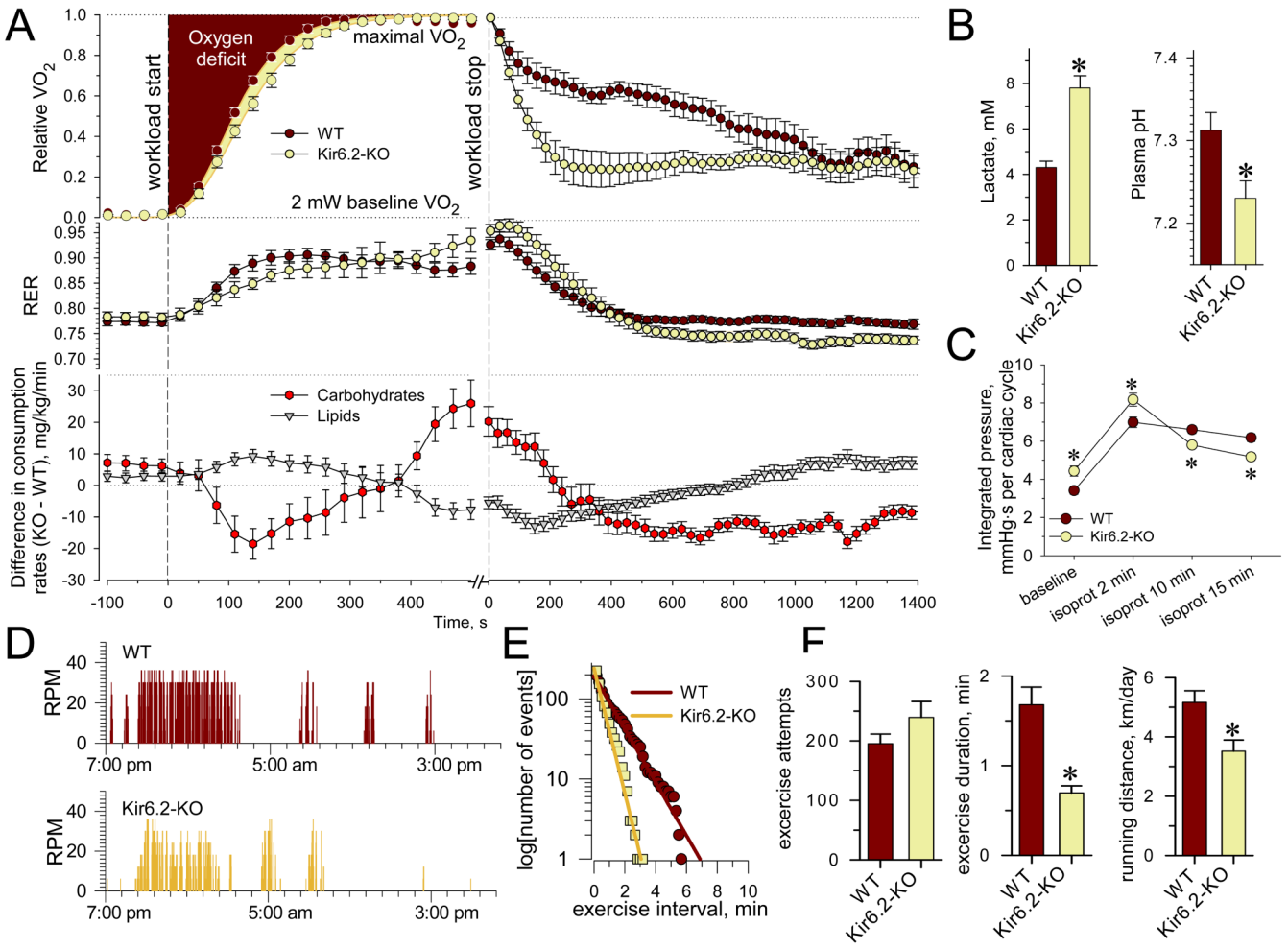

Figure 6. Reduced endurance and voluntary performance in Kir6.2-KO

(A) Relative VO_2 (*upper trace*) and RER (*middle trace*) in WT (n=10) and Kir6.2-KO (n=11) were constructed during 30 mW treadmill workload and post-exercise recovery, respectively. The differences in KO versus WT in carbohydrate and lipid consumption rates are presented for corresponding time points (*lower trace*). Data points were acquired at 30 s intervals.

(B) Plasma lactate and pH measured in blood samples taken immediately upon exhaustion from Kir6.2-KO (n=4) and WT (n=5).

(C) In response to isoproterenol (10 μM), Kir6.2-KO hearts were not able to sustain the integrated LV pressure per cardiac cycle compared to WT hearts (n=7 in each group).

(D) Representative recordings of voluntary performance during 24 h in WT and Kir6.2-KO housed in cages with attached running wheels.

(E) Distributions of activity intervals were fitted by single exponential functions (lines on the semi-logarithmic scale). The higher exponential slope indicates a shortened mean exercise duration for Kir6.2-KO (0.56±0.02 min) *versus* WT (1.31±0.02 min).

(F) Analysis of distributions for WT (n=10) and Kir6.2-KO (n=11) revealed similar number of voluntary exercise attempts (first bin), yet the mean exercise duration was double in WT compared to Kir6.2-KO. Accordingly, the running distance, defined based on wheel circumference and RPM, was compromised in Kir6.2-KO.

Data are mean±SEM;*, $p<0.05$.

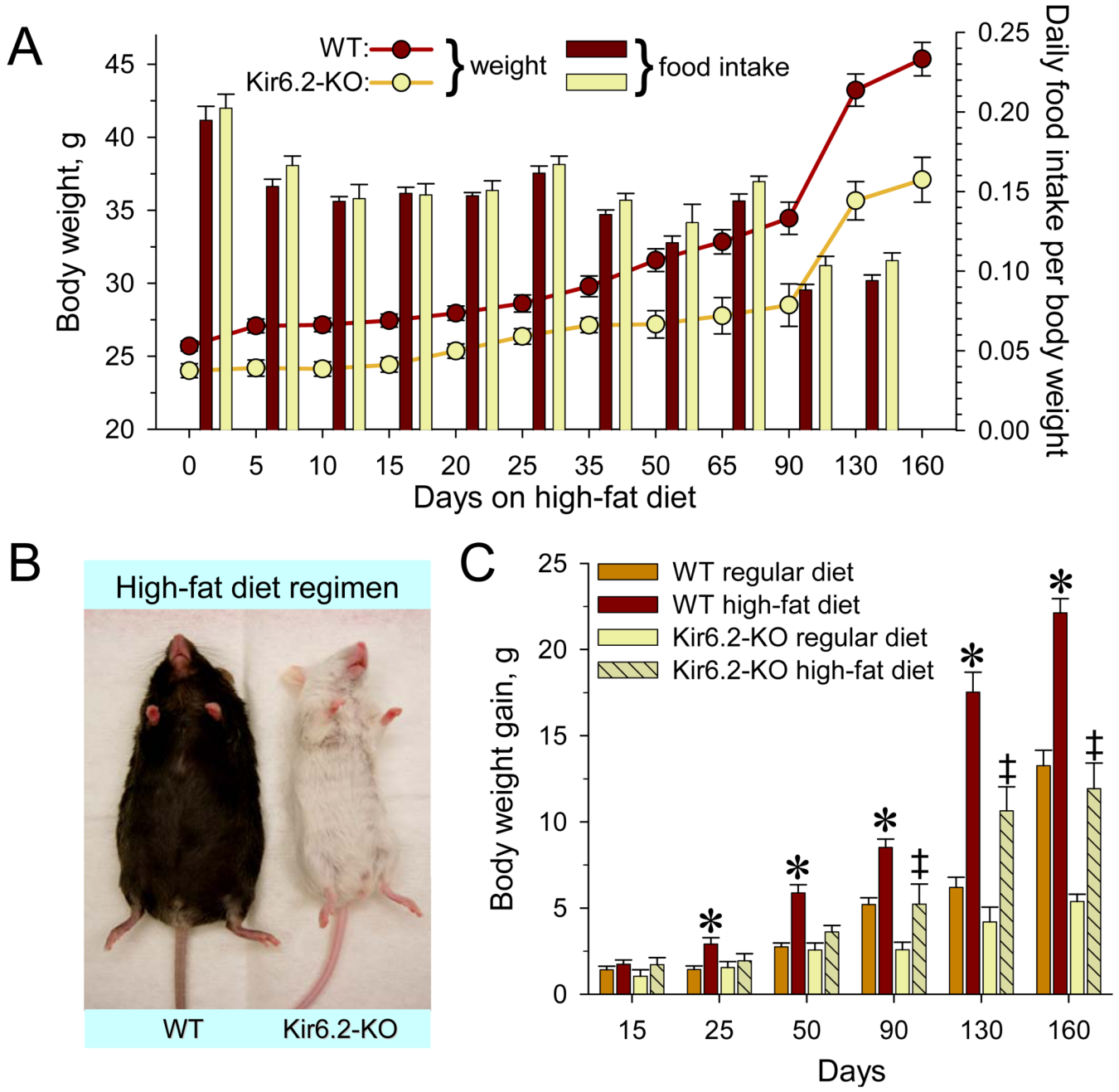

Figure 7. Resistance to high-fat diet induced obesity in Kir6.2-KO

(A) Under a high-fat diet regimen, Kir6.2-KO (n=10) gained less weight (*left y-axis*) than age- and gender-matched WT (n=10), despite comparable food consumption (*right y-axis*).

(B) Representative WT and Kir6.2-KO after 90 days of high-fat diet regimen.

(C) High-fat diet accelerated the rate of weight gain compared to regular chow diet in both WT and Kir6.2-KO, as determined by linear regression. However, the weight gain in WT was significantly higher compared to regular diet already at 25 days of the high fat regimen (*, $p<0.05$, n=10 for both groups), in contrast to 90 days for Kir6.2-KO (‡, $p<0.05$, n=10 in each group). Furthermore, the weight gained by Kir6.2-KO throughout the high-fat diet regimen was considerably lower compared to WT.

Data are mean±SEM.